

Stellar neutron capture cross sections of Nd, Pm, and Sm isotopes

K.A. Toukan

College of Engineering and Technology, The University of Jordan, Amman, Jordan

K. Debus and F. Käppeler

Kernforschungszentrum Karlsruhe, Institut für Kernphysik, Postfach 3640 D-76021 Karlsruhe, Germany

G. Reffo

ENEA, Laboratorio Dati Nucleari, Viale Ercolani 8, I-40138 Bologna, Italy

(Received 28 September 1994)

The neutron capture cross sections of $^{146,148,150}\text{Nd}$ have been determined relative to that of gold by means of the activation method. The samples were irradiated in a quasistellar neutron spectrum for $kT = 25$ keV using the $^7\text{Li}(p,n)^7\text{Be}$ reaction near threshold. Variation of the experimental conditions in different activations and the use of different samples allowed for the reliable determination of corrections and the evaluation of systematic uncertainties. The resulting stellar cross sections can be given with uncertainties around 6%, which represents a considerable improvement compared to previous measurements. These data are complemented by a new set of calculated cross sections for the unstable isotopes ^{147}Nd , $^{147,148,149}\text{Pm}$, and ^{151}Sm , which act as branching points in the s -process path. Based on these results, the s -process flow in the Nd-Pm-Sm region is discussed with respect to the neutron density during stellar helium burning and to isotopic anomalies in meteorites. The updated s -abundances are also used for a discussion of r - and p -process residuals.

PACS number(s): 25.40.Lw, 25.70.Gh, 97.10.Cv, 27.60.+j

I. INTRODUCTION

The s -process abundance pattern in the Nd-Pm-Sm region has been investigated repeatedly [1–3] since it includes one of the major branchings in the neutron capture flow. These major branchings are characterized by two s -only isotopes. The importance of this feature is illustrated in Fig. 1. The s nuclei ^{148}Sm and ^{150}Sm are shielded against the β -decay chains from the r process by their stable neodymium isobars. Furthermore, the reaction flow of the s process (solid lines) is partly bypassing ^{148}Sm due to the sequence of branch point nuclei ^{147}Nd , ^{147}Pm , ^{148}Pm , and ^{149}Pm . Since the abundance of the second s -only isotope ^{150}Sm is determined by the entire reaction flow, the local approximation — that the product of stellar neutron capture cross section (σ) and s -process abundance N_s is constant for neighboring isotopes [4] — is violated. The respective difference reflects the combined effect of the branchings between ^{147}Nd and ^{149}Pm , and is mainly determined by the neutron density during the s process.

In a first investigation by Winters *et al.* [1], the effective branching factor was determined to be

$$f_{-}^{\text{eff}} \approx \frac{\langle \sigma \rangle N_s(^{148}\text{Sm})}{\langle \sigma \rangle N_s(^{150}\text{Sm})} = 0.91 \pm 0.03, \quad (1)$$

but the interpretation of this result in terms of the neutron density remained ambiguous since the level scheme of ^{148}Pm was too uncertain for determining its stellar

decay rate. This problem has been solved by Lesko *et al.* [2], who showed that the isomer ($t_{1/2} = 41.3$ d) and ground state ($t_{1/2} = 5.37$ d) were in thermal equilibrium for $T_8 > 1.5$, suggesting an effective s -process neutron density of $n_n = (3.1 \pm 1.2) \times 10^8 \text{ cm}^{-3}$.

Since most of this uncertainty was due to the uncertainty of the branching factor f_{-}^{eff} and hence to the cross section ratio of the two s -only isotopes, this ratio was measured with improved accuracy by Wisshak *et al.* using the Karlsruhe $4\pi\text{BaF}_2$ detector [3]. Employing their result, $f_{-}^{\text{eff}} = 0.87 \pm 0.01$, the mean s -process neutron density could be given as $n_n = (3.8 \pm 0.6) \times 10^8 \text{ cm}^{-3}$.

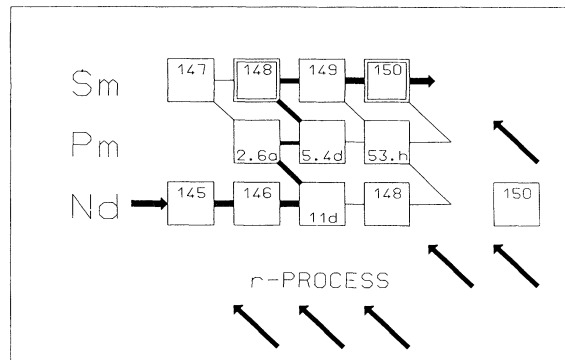


FIG. 1. Nucleosynthesis in the Nd-Pm-Sm region with the s -process branchings at $A=147$, 148, and 149.

The remaining uncertainty of this analysis is no longer dominated by the cross section ratio of the s -only nuclei. Apart from possible (but small) p -process corrections to the abundances of ^{148}Sm and ^{150}Sm , the (n, γ) cross sections of the unstable branch point isotopes are the most critical quantities.

These cross sections had been adopted from statistical model calculations based on a carefully evaluated parameter systematics [1]. The results of these calculations were estimated to exhibit uncertainties of typically 25%. The first attempt to measure the cross section of ^{147}Pm indicated a much lower value [5], almost a factor of 2 smaller than the calculated cross section. Unfortunately, this experiment suffered from the fact that the ^{147}Pm sample was contaminated with a ^{146}Pm impurity, leading to intricate difficulties in the analysis.

In this situation, the aim of the present work was three-fold:

(i) To remeasure the cross sections of the stable neodymium isotopes ^{146}Nd and ^{148}Nd , which are part of the branchings under discussion. Previous measurements of these data [6–15] exhibit large discrepancies of up to a factor of 3, despite the quoted uncertainties, which are typically 10–15%. For completeness, the r -process nucleus ^{150}Nd was investigated as well in order to check the cross section trend with neutron number starting from the closed shell at $N = 82$ (Secs. II, III).

(ii) To update and to improve the parameter systematics for the statistical model calculations, aiming at a new set of cross sections for the unstable branch point isotopes (Sec. IV).

(iii) To discuss the resulting consequences for the interpretation of the abundance pattern in the Nd-Pm-Sm region, in particular with respect to the s -process neutron density, but also for the discussion of isotopic anomalies in meteorites and the r - and p -process residuals close to the r -process abundance peak at $A = 130$ (Sec. V).

II. EXPERIMENTAL TECHNIQUE AND ACTIVATIONS

For the determination of the stellar neutron capture cross sections of ^{146}Nd , ^{148}Nd , and ^{150}Nd , samples of natural elemental neodymium were irradiated in a quasi-stellar neutron spectrum. The experimental setup was the same as that described by Beer and Käppeler [16], with the samples directly attached to the respective neutron targets. The neutron spectrum is obtained by bombarding thick metallic lithium targets with protons of 1912 keV, 31 keV above the reaction threshold. The $^7\text{Li}(p, n)^7\text{Be}$ reaction then yields a continuous neutron energy distribution with a high energy cutoff at $E_n = 106$ keV. It has been shown that the resulting neutrons are emitted in a forward cone of 120° opening angle. The angle-integrated spectrum peaks at 25 keV and exhibits almost exactly the shape required to determine the proper cross section average $\langle \frac{\sigma v}{v_T} \rangle$ corresponding to the stellar cross section for a thermal energy of $kT = 25 \pm 0.5$ keV [17]. Hence, the reaction rate measured in such a spectrum yields immediately the stellar cross section.

Before each activation, the correct proton beam energy was verified experimentally by a time-of-flight (TOF) measurement of the respective maximum neutron energy of 106 keV. The accelerator was then switched from a pulsed to dc mode without changing the proton energy. Throughout all activations the neutron yield was continuously monitored over 0.01 and 2 min intervals, for short and long irradiations, respectively, for later correction of the total sample activity due to changes in the neutron flux. After the irradiations, the samples were removed from the accelerator for activity determination in a low background environment using a HP-Ge detector. The peak-to-Compton ratio of the detector is 32 and the energy resolution is 1.7 keV at a gamma-ray energy of 1.33 MeV. The detector efficiency ϵ_γ was carefully calibrated in the range $150 < E_\gamma < 800$ keV using a set of standard sources [18]. The uncertainty in ϵ_γ in the energy region of the relevant Nd γ -ray lines is 2.0%.

The samples consisted of metallic neodymium disks of 10 mm diameter, which were directly placed on the lithium target. Since neodymium is one of the more reactive rare-earth metals and quickly tarnishes in air [19], the samples were always preserved in an argon atmosphere, during irradiation as well as during counting. The sample diameter is slightly smaller than the diameter of the neutron cone outside of the 1.5 mm thick copper backing (Fig. 2). Consequently, the effective sample thickness is given by the total mass, which was weighed to ± 0.1 mg.

In all activations, the neodymium samples were sandwiched between two 0.03 mm thick gold foils of the same diameter. These foils served for normalization to the well-known gold cross section, which was determined in an identical neutron spectrum to 648 ± 10 mb at $kT = 25$ keV [17]. This normalization accounts directly for the definition of the stellar cross section; to obtain the straight spectrum-averaged cross sections, the present results have to be multiplied by a factor $\frac{\sqrt{\pi}}{2}$ (for details see

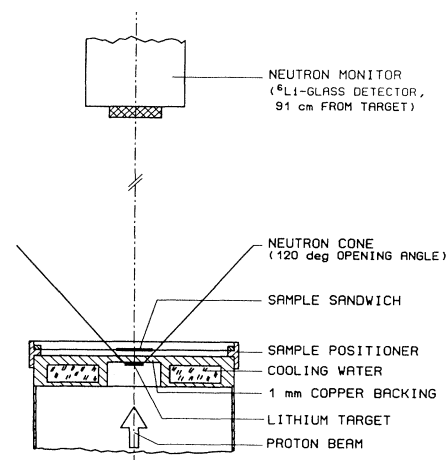


FIG. 2. Schematic sketch of the experimental setup during the activations. The scale along the symmetry axis is enhanced for illustrating the arrangement of the samples with respect to the neutron production target more clearly.

Ratynski and Käppeler [17]).

The characteristics of all samples used in the seven activations are summarized in Table I together with the respective activation schemes. To ensure maximum precision, the irradiation times t_b were chosen according to the half-lives of the investigated isotopes. For example, the ^{150}Nd cross section was determined via activations ND2, ND6, and ND7, which lasted for ~ 25 min. The induced ^{151}Nd activity ($t_{1/2} = 12.44$ min) was then immediately counted. However, the good sensitivity of the activation technique allowed also for collecting enough events from the decay of the longer-lived ^{149}Nd ($t_{1/2} = 1.72$ h), so that the ^{148}Nd cross section could be deduced from the same activations. Similarly, the cross sections for ^{146}Nd and ^{148}Nd could also be obtained simultaneously from activations ND3, ND5 ($t_b \sim 3.5$ h). In these cases, counting of the induced activities started with a delay of 30 min and several hours, respectively, to allow the shorter-lived isotopes to decay first. By the systematic variation of the experimental conditions with respect to sample thickness, irradiation time, and neutron flux, the respective uncertainties of the measurement could be studied and the corresponding corrections be determined reliably.

After the irradiations, the induced activities were measured for each sample separately. Figure 3 presents the γ -ray spectrum taken after irradiating a 0.1 mm thick

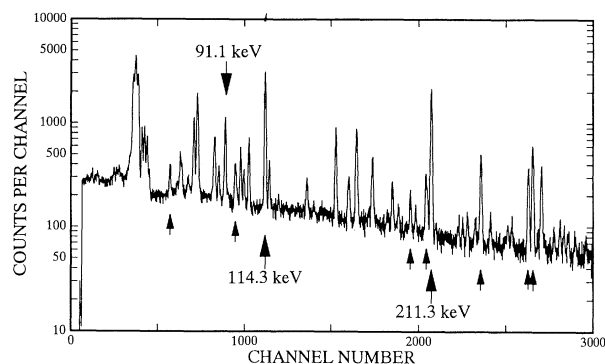


FIG. 3. The γ -ray spectrum measured after activation ND3 (0.102 keV per channel). The lines used for evaluation of the ^{146}Nd and ^{148}Nd cross sections are indicated by arrows (downward, decay of ^{147}Nd ; upward, decay of ^{149}Nd).

neodymium sample for 3.5 h (activation ND3). In addition to numerous lines from the decay of ^{149}Nd (upward arrows) the spectrum includes also the major line from the comparably long-lived ^{147}Nd (downward arrow) with sufficient statistical significance. The other lines are partly from the decay of the Pm daughters, partly from the decay of ^{151}Nd . The relevant γ -ray transitions used for evaluation of the respective cross sections are given with their energies. In all cases, these lines are characterized by favorable signal-to-background ratios, similar to the examples shown in Fig. 3. To verify proper background subtraction, the intensities of the 91.1 keV, 211.3 keV, and 116.8 keV lines were recorded as a function of time. The respective half-lives were found to agree with the values reported in the literature (Table II) within the statistical uncertainties of the measurement, thus excluding any significant contamination by unidentified background components. The gold activity was derived via the well-known 411.8 keV transition in ^{198}Hg . The decay parameters used in further analysis are listed in Table II [20–23].

TABLE I. Activation schemes and sample characteristics.

Run	Activations		Samples	
	Sample sequence ^a	Irradiation time	Thickness (mm)	Total mass (mg)
ND1	Au	65.3 h	0.03	49.1 \pm 0.1
	Nd (146) ^b		0.10	55.7 \pm 0.1
	Au		0.03	48.5 \pm 0.1
ND2	Au	24.8 min	0.03	47.9 \pm 0.1
	Nd ($^{148},^{150}$) ^b		0.10	55.4 \pm 0.1
	Au		0.03	48.0 \pm 0.1
ND3	Au	3.55 h	0.03	44.9 \pm 0.1
	Nd ($^{146},^{148}$) ^b		0.10	56.3 \pm 0.1
	Au		0.03	46.4 \pm 0.1
ND4	Au	44.3 h	0.03	48.8 \pm 0.1
	Nd (146) ^b		0.025	16.4 \pm 0.1
	Au		0.03	48.7 \pm 0.1
ND5	Au	3.50 h	0.03	46.8 \pm 0.1
	Nd ($^{146},^{148}$) ^b		0.05	32.1 \pm 0.1
	Au		0.03	45.7 \pm 0.1
ND6	Au	26.9 min	0.03	46.8 \pm 0.1
	Nd ($^{148},^{150}$) ^b		0.05	33.4 \pm 0.1
	Au		0.03	46.8 \pm 0.1
ND7	Au	26.4 min	0.03	46.9 \pm 0.1
	Nd ($^{148},^{150}$) ^b		0.10	55.7 \pm 0.1
	Au		0.03	46.9 \pm 0.1

^aThe first listed sample was closest to the neutron target.

^bInvestigated isotopes.

TABLE II. Decay properties of the relevant product nuclei.

Product nucleus	Half-life	Gamma-ray energy (keV)	Relative intensity per decay (%)
^{147}Nd	10.98 \pm 0.1 d	91.105	27.90 \pm 1.10 ^a
		531.016	13.08 \pm 0.89 ^a
^{149}Nd	1.72 \pm 0.01 h	211.309	25.90 \pm 1.44 ^b
		114.314	19.04 \pm 1.57 ^b
^{151}Nd	12.44 \pm 0.07 min	116.80	43.37 \pm 2.42 ^c
		255.68	16.43 \pm 0.94 ^c
^{198}Au	2.696 \pm 0.002 d	411.8	95.5 \pm 0.1 ^d

^aMateosian and Peker [20].

^bSzucs, Johns, and Singh [21].

^cSingh, Szucs, and Johns [22].

^dAuble [23].

III. ANALYSIS AND RESULTS

A. Data evaluation and systematic uncertainties

The net counts C_γ for each of the peaks in Fig. 3 can be expressed as

$$C_\gamma = A K_\gamma \epsilon_\gamma I_\gamma f_w f_m, \quad (2)$$

where A denotes the total number of activated nuclei at the end of irradiation, K_γ the gamma-ray self-absorption factor, ϵ_γ the efficiency of the HP-Ge detector, and I_γ the relative gamma-ray intensity per decay. The time factors $f_w = e^{(-\lambda t_w)}$ and $f_m = (1 - e^{(-\lambda t_m)})$ account for the fraction of nuclei that decay during the waiting time between irradiation and measurement and during the measurement itself, and are discussed elsewhere [16]; λ is the decay constant of the respective product nucleus. The corrections for γ -ray self-absorption, K_γ , were calculated with the absorption coefficients of Storm and Israel [24].

The total number of activated nuclei, A , is given by

$$A = \Phi_{\text{tot}} N \sigma f_b, \quad (3)$$

where $\Phi_{\text{tot}} = \int \Phi(t) dt$ is the time-integrated neutron flux, N the sample thickness, and σ the spectrum-averaged neutron capture cross section. The time factor f_b corrects for the decay during activation, including the effects due to the time dependence of the neutron flux (for a definition see Beer and Käppeler [16]). Since the neodymium cross sections are normalized to that of gold, corrections for target geometry as well as for neutron scattering and self-shielding cancel out. Hence, the

activity ratio in the respective target and reference samples is to very good accuracy given by

$$\frac{A_i}{A_{\text{Au}}} = \frac{\sigma_i N_i f_{b,i}}{\sigma_{\text{Au}} N_{\text{Au}} f_{b,\text{Au}}}. \quad (4)$$

The corresponding uncertainties are listed in Table III. In all cases, the total uncertainties of the resulting neodymium cross sections are clearly dominated by the contributions from the relative decay intensities I_γ . Therefore, further improvement of these quantities could reduce the uncertainties to about 3%, which corresponds to the combined uncertainties of the time factors, counting statistics, and self-absorption corrections.

Apart from the relative decay intensities, a significant uncertainty is introduced by the efficiency ratio for the Nd and Au γ -ray lines. The larger uncertainty of 2% for ^{146}Nd and ^{150}Nd is due to the fact that the respective lines fall below the energy region where the efficiency satisfies the simple relation $\ln \epsilon_\gamma = a + b \ln E_\gamma$. The flux Φ_{tot} , measured with the two gold foils, showed a systematic difference due to the divergent neutron field. The corresponding uncertainty was assumed to be 20% of this difference.

Due to the cutoff in the neutron spectrum at $E_n = 106$ keV, a correction is required for the possible difference in the cross section shape relative to gold at higher energies. A related problem is the extrapolation of the stellar cross sections from the investigated value of 25 keV to other thermal energies, in particular to $kT = 30$ keV, the standard thermal energy at which s -process cross sections are usually quoted. These corrections can be made with confidence only if the energy dependence of the investigated cross section is sufficiently well known. In case of the Nd

TABLE III. Compilation of uncertainties.

Source of uncertainty	Uncertainty (%)			
	Au	^{146}Nd	^{148}Nd	^{150}Nd
Gold cross section	1.5
Sample thickness	0.2	0.2	0.2	0.2
Time factors f_w, f_m, f_b	<0.4	<0.5	<0.5	<0.9
Counting statistics	<0.9	<1.5	<2.0	<1.3
Self-absorption K_γ	0.03	<1.2	<0.1	<0.8
Efficiency ratio for Nd and Au gamma-ray lines	...	2.0	1.5	2.0
Gamma-ray intensity per decay, I_γ	0.1	3.9	5.6	5.6
Difference in neutron flux	...	<1.5	<1.5	<1.5
Spectrum cutoff at 106 keV	...	0.3	0.3	0.3
Total uncertainty ($kT = 25$ keV)				
ND1	...	4.6
ND2	6.1	6.1
ND3	...	4.7	6.0	...
ND4	...	4.5
ND5	...	5.0	6.0	...
ND6	6.1	6.1
ND7	6.0	6.0
Extrapolation to $kT = 20$ and 30 keV	...	0.8	0.8	1.2
Extrapolation to $kT = 12$ and 52 keV	...	4.0	3.0	5.0

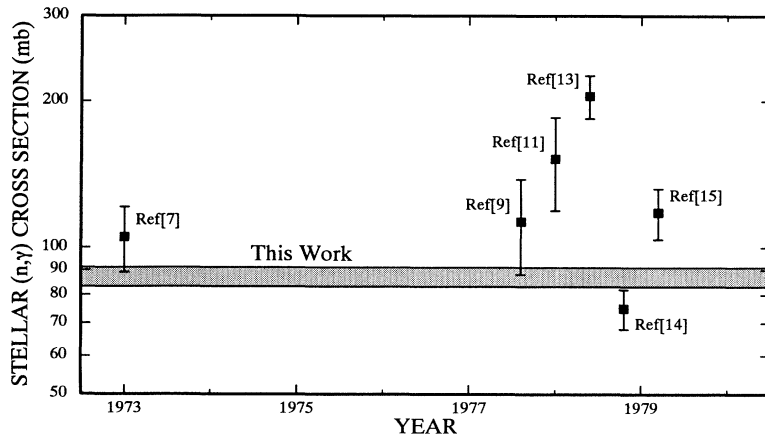


FIG. 4. Comparison of the new stellar ^{146}Nd cross section for a thermal energy of $kT = 30$ keV with previous experimental data.

isotopes, such data are available for all naturally existing isotopes. However, there are significant discrepancies between the available data sets in the relevant energy region from 1 keV to 500 keV neutron energy [9,11,13,15].

Therefore, these corrections were evaluated by means of the eye-guided curves in the cross section compilation of McLane, Dunford, and Rose [25]. The resulting corrections for the spectrum cutoff were 1% for ^{146}Nd and ^{148}Nd , and 0.5% for ^{150}Nd . The respective uncertainties

were assumed to be 0.3% in all cases. The uncertainties for the extrapolation to other thermal energies will be discussed below.

B. Experimental cross sections

The present results from all activations are summarized in Table IV together with the final averages and

TABLE IV. Stellar neutron capture cross sections of ^{146}Nd , ^{148}Nd , and ^{150}Nd compared with previous data.

Thermal energy (keV)	$\frac{\langle\sigma v\rangle}{vT}$ (mbarn)		
	^{146}Nd	^{148}Nd	^{150}Nd
	Previous data		
30	150 ^a	210±80 ^a	240±150 ^a
	105±16 ^b	221±40 ^b	...
	113±25 ^c	123±20 ^c	...
	152±33 ^d	208±26 ^d	...
	205±21 ^e	186±19 ^e	187±19 ^e
	75±7 ^f	99.4±14 ^f	...
	118±14 ^g	130±15 ^g	153±18 ^g
	102 ^h	82 ^h	147 ^h
	104 ⁱ	216 ⁱ	262 ⁱ
	This work		
25	ND1	97.1±4.5	...
	ND2	...	170±10
	ND3	93.4±4.4	164±10
	ND4	92.6±4.2	...
	ND5	100.0±5.4	162±10
	ND6	...	169±11
	ND7	...	171±10
	Mean value	95.4±4.6	166±10
30	87.1±4.0	152±9	159±10

^a Allen *et al.* [6].

^b Siddappa *et al.* [7], from Conrad [8].

^c Musgrove *et al.* [9], $k = 0.9833$ [10].

^d Nakajima *et al.* [11], from Mathews and Käppeler [12].

^e Kononov *et al.* [13].

^f Bradley *et al.* [14].

^g Iijima *et al.* [15].

^h Holmes *et al.* [28].

ⁱ Harris [29].

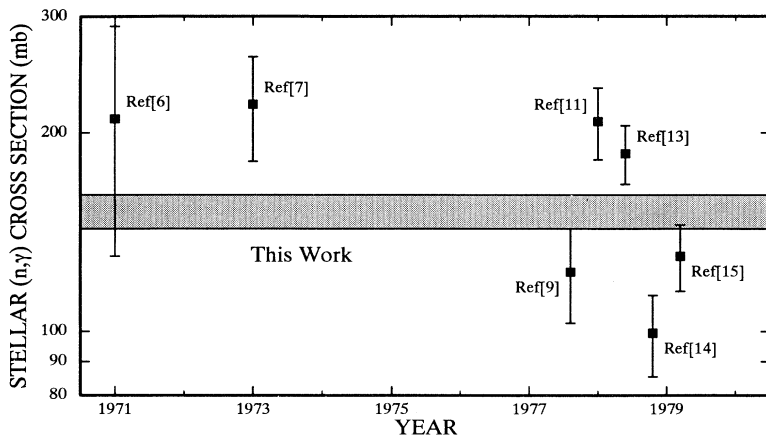


FIG. 5. Comparison of the new stellar ^{148}Nd cross section for a thermal energy of $kT = 30$ keV with previous experimental data.

previous data. Since the uncertainties are by far dominated by systematic effects, the final cross sections were not considered to be more accurate than the results from the individual runs. However, the comparison of the various activations shows that the observed scatter around the mean is compatible with the uncorrelated uncertainties, indicating that the various corrections were properly considered.

For the extrapolation to other thermal energies, the energy dependence of the various cross sections was adopted from the literature [25], assuming that the cross section shapes should be more reliable than the absolute values. The resulting correction factors were compared with those obtained with a $1/v$ dependence of the cross section, and $1/3$ of that difference was adopted as an estimate of the corresponding uncertainties (Table III).

The comparison with previous data for $kT = 30$ keV in Figs. 4 and 5 shows that the experimental uncertainties could at least be reduced by a factor of 2. Even more important, the present results allow one to rule out those cross section values which caused the unacceptable discrepancies in the previous data. The most extreme example is the cross section of ^{146}Nd . The existing information was summarized to a recommended stellar value of 157 ± 40 mbarn at 30 keV [26,27], whereas the present result of 87.1 ± 3.7 mbarn is a factor of 2 smaller. This difference implies an increase of the s abundance by a factor of 2. For ^{148}Nd and ^{150}Nd there is better agreement with the compiled values (20% and 15%, respectively), but with similar reductions of the uncertainties.

Part of these discrepancies in the previous data might have been due to the specific techniques used. For example, the measurement of Bradley *et al.* [14] was also made with the activation technique, but using a filtered neutron beam at a nuclear reactor. In this case, the neutron spectrum was limited to a narrow window of $E_n = 24 \pm 2$ keV. Accordingly, the results are sensitive to fluctuations in the cross section. Hence, their generalization for a stellar spectrum can bear large uncertainties as observed for ^{148}Nd . Another discrepancy by a factor of 2 occurs in the data of Kononov *et al.* [13] for ^{146}Nd . While most other previous cross sections are in reasonable agreement with the present results (within their rather large uncer-

tainties), the latter two values should be discarded from further consideration.

The discrepancies between the present data and the results of previous statistical model calculations (Holmes *et al.* [28] and Harris [29]) are compatible with the 50% uncertainty typical for the quality of these approaches with global parameter sets (see Sec. IV).

IV. STATISTICAL MODEL CALCULATIONS

The discrepancy between the results of existing statistical model calculations for the cross sections of the radioactive branch point nuclei [28,29] and the progress achieved meanwhile in determining the relevant model parameters prompted the update presented here.

The methodology of the calculations (evaluation of a consistent set of model parameters from a *local* systematics preferentially based on experimental data) was discussed for the Nd-Pm-Sm region in detail in a previous paper [1]. Meanwhile, new information from neutron resonance analyses became available, which were performed in the frame of an IAEA-coordinated research program [30]. By combination of three independent analyses the parameter set could be significantly improved.

On this basis, detailed Hauser-Feshbach calculations including the superelastic channel were carried out using the modular system of codes IDA [31–33]. With respect to (n, γ) cross sections, this formalism is sensitive to the parameters characterizing the compound nucleus, such as the level density parameter a , the radiative width Γ_γ , and only to a minor extent to the optical model parameters describing the entrance channel. This means that the relevant input data for such calculations can be derived from neutron resonance schemes. These yield the mean level spacings, which can be combined with the discrete level schemes to obtain a reliable description of the level density in the compound system. Furthermore, also the mean radiative widths and the strength functions S_0 and S_1 can be deduced, which are useful for the cross section calculations and for the parametrization of the optical model, respectively.

TABLE V. Level density parameters for the compound nuclei.

Compound nucleus	E_{cut} (MeV)	a (MeV ⁻¹)	U_x (MeV)	σ^2	β^a	S_0	S_1	D_{obs} (eV)	$\Gamma_{\gamma}^{\text{expt}}$ (meV)	$\Gamma_{\gamma}^{\text{calc}}$ (meV)
¹⁴⁸ Nd	1.3	24.9	4.5	4.0	0.192	5.4	1.3	4.9±1.5	50 ^b	44±12
¹⁴⁷ Pm	0.34	20.0	5.3	6.6	0.151	3.36	...	100±30
¹⁴⁸ Pm	0.214	21.2	3.6	7.9	0.179	3.3±0.7	1.6	6.0	69±15 ^c	58±17
¹⁴⁹ Pm	0.53	23.0	5.2	9.1	0.198	5.4	1.6	1.12	...	58±16
¹⁵⁰ Pm	0.20	23.8	5.5	8.5	0.212	67
¹⁴⁷ Sm	0.30	20.8	4.3	5.9	0.131	75
¹⁴⁸ Sm	1.43	20.8	4.3	5.9	0.151	4.8±0.5	...	6.8±0.8	69±2 ^c	64
¹⁴⁹ Sm	0.59	23.8	4.7	8.4	0.171	5.4	1.3	108 ^d	...	70
¹⁵⁰ Sm	1.45	23.5	4.8	6.2	0.198	4.6±0.6	1.25	2.5±0.5	62±2 ^c	52
¹⁵¹ Sm	0.296	26.9	5.5	6.5	0.205	56 ^d	60±5 ^c	56
¹⁵² Sm	0.81	24.1	5.4	8.3	0.225	4.1±0.5	...	1.4±0.4	92±7 ^c	67
¹⁵³ Sm	0.938	24.7	5.5	8.3	0.225	2.15±0.03	...	46±7	61±7 ^c	...

^aReference [34].

^bPresent analysis based on Ref. [35].

^cPresent analysis based on Ref. [36].

^dAdopted from a systematics.

A. Evaluation of model parameters

Although the systematics reported previously [1] was confirmed in general, changes were required for the level density parameters of the Nd and Pm isotopes, whereas small modifications with respect to deformations [34] and strength functions were sufficient for the Sm isotopes (for details compare Table V with Table X of Winters *et al.* [1]). Table V provides also a comparison between calculated and experimental values for the mean radiative widths [35,36].

The case of ¹⁴⁷Pm deserves a more detailed discussion, because it can be measured experimentally [5,37], hence

representing an important test for the calculations. One of the problems in evaluating the average resonance parameters of ¹⁴⁸Pm is that only 11 resonances are known for this isotope. Therefore, it is difficult to derive these parameters by common statistical techniques. If this uncertainty is taken into account, the observed level spacing D_{obs} ranges between 4 and 7 eV. Given the uncertainties of the other relevant parameters, the calculated cross sections were expected to show a large uncertainty of ~50%. On the other hand, the extremes of 4 and 7 eV would translate to values for a , U_x , and T , which are incompatible with the respective systematics. On these grounds, it is plausible to adopt $D_{\text{obs}} = 5 \pm 1$ eV, which corresponds

TABLE VI. Calculated (n, γ) cross sections.

Neutron energy (keV)	Target nucleus								
	¹⁴⁷ Nd	¹⁴⁷ Pm	¹⁴⁸ Pm	¹⁴⁹ Pm	¹⁴⁷ Sm	¹⁴⁸ Sm	¹⁴⁹ Sm	¹⁵⁰ Sm	¹⁵¹ Sm
1	6780	11730	16600	16050	10100	1750	16060	3590	24430
5	1880	3220	4200	4000					6850
10	1090	1890	2870	2700	1640	340	2690	590	4030
15	825	1425	2150	2000					2950
20	700	1200	1770	1650	1040	240	1650	410	2400
25	605	1030	1505	1420					2000
30	550±150	950±250	1380±350	1280±320	820	200	1170	345	1825±450
40	470	805	1180	1080					1500
50	420	725	1050	960	620	170	860	290	1340
70	312	600	830	830					960
100	235	500	670	700	460	150	610	255	680
150	155	415	520	570					465
200	121	365	450	500	320	140	480	245	355
300	85	315	300	300					240
400	67	290	225	230	220	130	330	145	180
600	49	250	200	180					142
$\left(\frac{\langle \sigma v \rangle}{v_T}\right)_{30 \text{ keV}}$	550	985	1410	1345	860	225	1270	385	1820
$\left(\frac{\langle \sigma v \rangle}{v_T}\right)_{30 \text{ keV}}^a$	973±10	241±2	1820±17	422±4	...

^aExperimental values from Ref. [3].

TABLE VII. Stellar (n, γ) cross sections $\left(\frac{\langle\sigma v\rangle}{v_T}\right)$ (mbarn) .

Thermal energy (keV)	Target nucleus							
	^{146}Nd	^{147}Nd	^{148}Nd	^{150}Nd	^{147}Pm	^{148}Pm	^{149}Pm	^{151}Sm
12	164±11	1033	225±15	308±23	1750	2520	2375	3580
20	110±5	729	178±11	209±12	1260	1820	1710	2470
25	95.4±4.6	625	166±10	174±11	1095	1580	1495	2100
30	87.1±4.0	550±150	152±9	159±10	985±250	1410±350	1345±320	1820±450
40	79.1±3.4	449	138±9	132±8	835	1175	1135	1460
52	69.8±3.2	370	125±9	111±7	720	995	980	1185

to a total uncertainty of $\sim 25\%$ for the calculated (n, γ) cross section of ^{147}Pm .

It should be noted that the spin and parity assignments of the discrete levels above the isomer are rather uncertain. The corresponding uncertainty refers mainly to the calculation of the isomeric ratio. However, this aspect is no longer important for this work, since the isomer and ground state are already equilibrated at all plausible s -process temperatures [2,38]. Therefore, the calculation of the isomeric ratio was not repeated.

B. Calculated cross sections

The calculated cross sections are summarized in Table VI. Comparison with the experimental results for the stable samarium isotopes [3] shows agreement within 20% on average, indicating that the estimated uncertainty of 25% was reasonable. On the other hand, Table VI also illustrates the limit of the statistical model. If compared with the previous set of calculated cross sections [1], one finds that the present results are lower by an almost constant fraction of $15\pm 5\%$, and that the previous data fit even better to the experimental cross sections. Apart from the absolute values, both calculations agree with respect to the cross section shape.

It appears, however, that the calculations are considerably more reliable in reproducing the correct trend of the stellar cross sections with neutron number. For this reason, an experimental value for the ^{147}Pm cross section would be most welcome. Such a measurement is certainly feasible, although a first attempt was hampered by an isotopic impurity from ^{146}Pm [5].

Since it is difficult to claim a preference for one of the two calculations, it is important to emphasize the persisting uncertainty of typically 25%. Therefore, all calculated Maxwellian average cross sections listed in Table VII are explicitly given with the individual uncertainties derived from a sensitivity study.

V. ASTROPHYSICAL ASPECTS

A. s -process neutron density

The neutron capture flow through the branchings at $A = 147\text{--}149$ has been analyzed with the new set of

Maxwellian averaged cross sections listed in Table VII and the corresponding data for the samarium isotopes [3].

For the present case, the branching analysis with the classical approach has been presented in detail in Ref. [1]. As in Ref. [3], this scheme was complemented by including the (minor) branch point isotope ^{149}Pm , and the empirical ratio of the $\langle\sigma\rangle N_s$ values of ^{148}Sm and ^{150}Sm was decreased by 0.4% to account for the calculated p -process yields of these isotopes [39–41]. The mean neutron density derived from this branching is found to be

$$n_n = (4.1 \pm 0.6) \times 10^8 \text{ cm}^{-3}.$$

This value is 8% higher than the $(3.8 \pm 0.6) \times 10^8 \text{ cm}^{-3}$ obtained by Wisshak *et al.* [3] using an older set of calculated cross sections for the unstable branch point isotopes [1]. Though the two results are in good agreement, the difference occurred obviously because the new cross sections are systematically lower.

In view of the fact that the difference between the theoretical data sets seems to represent the inherent uncertainty of such statistical model calculations, it is important to note that two-thirds of the respective difference in the deduced neutron density are due to ^{147}Pm . Using the upper limit for this cross section yields $n_n = 3.9 \times 10^8 \text{ cm}^{-3}$. Since this cross section can be determined experimentally with an uncertainty of less than 10% (for similar cases see Ref. [42]), there is the possibility for further substantial improvement in evaluating the mean s -process neutron density within the classical approach.

The branchings at $A = 147\text{--}149$ have also been investigated by means of a stellar s -process model. The helium-shell-burning episodes in thermally pulsing AGB stars in the mass range $1 < M/M_\odot < 3$ have been shown to provide the exponential distribution of neutron exposures characteristic of the *main s*-process component [43,44]. Accordingly, this scenario allowed us to reproduce the overall s -process abundance pattern between Zr and Bi to better than 10% [38,45,46]. Since two neutron sources, the $^{13}\text{C}(\alpha, n)^{16}\text{O}$ reaction and the $^{22}\text{Ne}(\alpha, n)^{25}\text{Mg}$ reaction, are active in that scenario at different times and temperatures, the s -process branchings represent a particularly sensitive test for this model.

Therefore, a similar comparison was made as for the classical approach, using the previous set of cross sections for ^{146}Nd , ^{148}Nd , and the branch point nuclei [1] and the

TABLE VIII. *s*-, *r*-, and *p*-process abundances between ^{142}Nd and ^{150}Sm .

Isotope	Solar abundance ^a		Classical approach			Stellar model
	$N_{\odot} \times 10^2$	$\langle \sigma \rangle N_s^b$	$N_s \times 10^2$	$N_r \times 10^2$	$N_p \times 10^2$	$N_s \times 10^2$
^{142}Nd	22.5±0.29	9.375	20.69±1.74	...	1.8±1.8	20.35
^{143}Nd	10.0±0.13	8.722	3.65±0.14	6.35±0.73	...	3.83
^{144}Nd	19.7±0.26	8.600	7.96±0.41	11.74±1.5	...	8.30
^{145}Nd	6.87±0.09	8.338	1.72±0.35	5.15±0.6	...	1.83
^{146}Nd	14.2±0.18	8.281	9.51±0.44	4.69±0.44	...	8.58
^{148}Nd	4.77±0.06	0.556	0.37±0.07	4.40±0.07	...	0.30
^{150}Nd	4.67±0.06	4.67±0.06
^{147}Sm	3.99±0.05	1.231	(0.88±0.18) ^c	3.11±0.19	...	0.77
^{147}Pm	...	6.451
^{147}Nd	...	0.568
^{148}Sm	2.92±0.04	7.053	(2.91±0.05) ^c	3.02
^{148}Pm	...	0.529
^{149}Sm	3.56±0.05	8.085	(0.45±0.01) ^c	3.11±0.07	...	0.42
^{149}Pm	...	0.038
^{150}Sm	1.91±0.02	8.060	1.91±0.03	1.91

^aFrom Ref. [49].

^bNormalized at ^{150}Sm .

^cIncluding the decay of isobars.

new set listed in Table VII. As before, the branching was defined via the samarium cross sections of Ref. [3]. The calculations were carried out with the network code NETZ [47] using the effective profiles for neutron density and temperature of the stellar model [48]. With the old set of data, ^{148}Sm was overproduced by 6% with respect to its solar abundance [49]. The corresponding calculation using the cross sections of this work yields a reduced but still significant overproduction of 3.4%. (Note that the uncertainties of N_s quoted in Table VIII refer to *absolute* values, but that the ratio $^{148}\text{Sm}/^{150}\text{Sm}$ carries only the 1% uncertainty of the cross section ratio.)

At first, this result appears as a surprise. Since the new cross sections for the branching points are systematically smaller, one would expect the mass flow bypassing ^{148}Sm to be enhanced, resulting in an increasing overproduction of this isotope. Closer inspection shows, however, that the better agreement with the observed ^{148}Sm abundance results from the significantly smaller ^{146}Nd cross section determined in this work, reflecting the stepwise freeze-out of the *s* abundances when the

neutron density declines at the end of the He-burning episodes. In the considered mass range, freeze-out occurs first at ^{146}Nd whereas the larger cross sections of the following isotopes allow one to maintain the reaction flow for some time. The next isotope, where freeze-out occurs, is ^{150}Sm . Therefore, the remaining reaction flow accumulates at this point, leading to a reduction of the abundance ratio $N_s(^{148}\text{Sm})/N_s(^{150}\text{Sm})$.

B. Isotopic anomalies

Isotopic anomalies in Nd were first detected in an acid resistant residue of the Allende meteorite by Lugmair *et al.* [50] and interpreted as being due to *s*-process Nd by Clayton [51]. While this work deals with anomalies of a few parts in 1000, much larger effects were observed by Zinner *et al.* [52] and by Richter *et al.* [53,54] in silicon carbide grains from the Murchison meteorite.

This anomalous abundance pattern in meteoritic SiC [53],

$$^{142}\text{Nd}/^{143}\text{Nd}/^{144}\text{Nd}/^{145}\text{Nd}/^{146}\text{Nd}/^{148}\text{Nd}/^{150}\text{Nd}$$

$$= 2.13 \pm 0.08/0.293 \pm 0.006/ \equiv 1/0.161 \pm 0.005/0.775 \pm 0.009/0.0281 \pm 0.0058/ \equiv 0$$

is compared in Fig. 6 with the *s*-abundances obtained in this work,

$$2.60 \pm 0.25/0.46 \pm 0.03/ \equiv 1/0.216 \pm 0.046/1.19 \pm 0.08/0.046 \pm 0.009/ \equiv 0.$$

Though the overall trend with mass number is very similar, the remaining differences are significantly larger than the respective uncertainties.

At present, it is difficult to make conclusions about

this situation. It is conspicuous, however, that the relative differences between the two abundance sequences are fairly constant around 30%. This may point to a problem with the normalization at ^{144}Nd . If the stellar

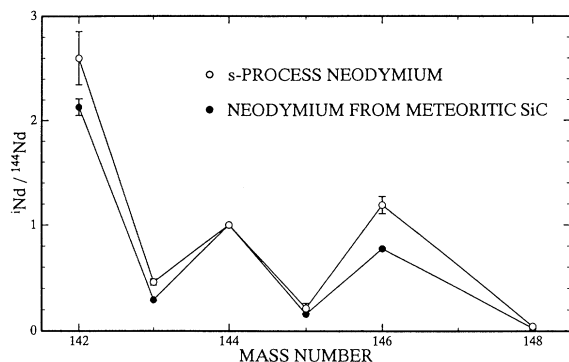


FIG. 6. Composition of s -process neodymium with the anomalous abundance pattern reported for SiC inclusions in the Murchison meteorite [54].

cross section of ^{144}Nd were too large by that factor, the meteoritic pattern could well be interpreted as pure s -process material. Normalization at ^{146}Nd , for which the cross section is presumably better known, yields good agreement for all isotopes, except for ^{142}Nd and ^{144}Nd . In that case, even the branching to ^{148}Nd is described consistently, in agreement with the neutron density deduced above via the s -only isotopes ^{148}Sm and ^{150}Sm . Hence, more accurate cross sections for the Nd isotopes are highly desirable.

C. r - and p -process residuals

The cross sections determined in this work were used to derive the r -process residuals in the mass range $146 < A < 150$ (Table VIII). These data contribute to a better characterization of the r -process abundance peak at $A = 130$ as shown in Fig. 7. Open symbols denote the r -process yields of Käppeler *et al.* [55] updated by the recent studies in Refs. [56,57]. In the case of the even isotopes (squares), these data exhibit rather large deviations from the generally observed smoothness between mass number $A = 142$ and 146. In the case of ^{146}Nd , the smaller cross section of this work led to an increase of the s -process contribution. Correspondingly, the r -process abundance is significantly reduced and fits much

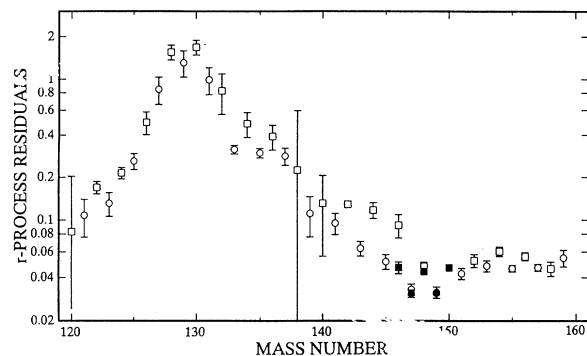


FIG. 7. r -process abundance peak at mass number $A=130$. Values from the present analysis are indicated by solid symbols; open symbols refer to the results of Ref. [55] updated by the work of Refs. [56,57]. The significant difference for ^{146}Nd is the consequence of the improved stellar cross section, which results in a correspondingly larger s abundance.

better to a smooth r -process pattern.

While the remaining excess at $A = 142$ may be due to a previously neglected branching of the s -process path at ^{141}Ce , the large r abundance of ^{144}Nd could result from a similar problem as for ^{146}Nd . The possibility of a smaller (n, γ) cross section for ^{144}Nd , as discussed in context with the observed isotopic anomalies, would also reduce the r abundance quoted in Table VIII.

For ^{142}Nd , the difference $N_{\odot} - N_s = 0.018 \pm 0.018$ (Table VIII) represents the p -process abundance since the r -process yield at $A = 142$ is accumulated by the stable isobar ^{142}Ce . This corresponds to a p -process contribution of 8% in qualitative agreement with recent model calculations [39–41]. A quantitative discussion, however, would require a significantly improved ^{142}Nd cross section.

ACKNOWLEDGMENTS

We thank A. Ernst, E.P. Knaetsch, D. Roller, and W. Seith for their help and support during the neutron irradiations at the Van de Graaff accelerator as well as G. Rupp for his excellent technical assistance throughout the entire experiment. The financial support of DAAD is gratefully acknowledged by one of us (K.A.T.).

- [1] R. Winters, F. Käppeler, K. Wisshak, A. Mengoni, and G. Reffo, *Astrophys. J.* **300**, 41 (1986).
- [2] K. Lesko, E. Norman, R.-M. Larimer, J. Bacelar, and E. Beck, *Phys. Rev. C* **39**, 619 (1989).
- [3] K. Wisshak, K. Guber, F. Voss, F. Käppeler, and G. Reffo, *Phys. Rev. C* **48**, 1401 (1993).
- [4] K. Wisshak, F. Voss, F. Käppeler, and G. Reffo, *Phys. Rev. C* **45**, 2470 (1992).
- [5] T. Gerstenhöfer, F. Käppeler, K. Wisshak, and G. Reffo, in *Nuclear Data for Science and Technology, Research Reports in Physics*, edited by S. Qaim (Springer, Berlin, 1992), p. 632.
- [6] B. J. Allen, J. H. Gibbons, and R. L. Macklin, *Adv. Nucl. Phys.* **4**, 205 (1971).
- [7] K. Siddappa, M. Sriramachandra Murty, and J. Rama Rao, *Nuovo Cimento A* **18**, 48 (1973).
- [8] J. Conrad, Ph.D. thesis, University of Heidelberg, 1976.
- [9] A. de L. Musgrove, B. Allen, J. Boldeman, and R. Macklin, in *Neutron Physics and Nuclear Data for Reactors and other Applied Purposes* (OECD, Paris, 1978), p. 449.
- [10] B. J. Allen, J. W. Boldeman, and R. L. Macklin, *Nucl. Sci. Eng.* **82**, 230 (1982).
- [11] Y. Nakajima, A. Asami, Y. Kawarasaki, Y. Furuta, T. Yamamoto, and Y. Kandou, in *Neutron Physics and Nuclear Data for Reactors and other Applied Purposes* (OECD, Paris, 1978), p. 438.
- [12] G. Mathews and F. Käppeler, *Astrophys. J.* **286**, 810 (1984).

- [13] V. Kononov, B. Yurlov, E. Poletaev, and V. Timokhov, *Yad. Fiz.* **27**, 10 (1978) [*Sov. J. Nucl. Phys.* **27**, 5 (1978)].
- [14] T. Bradley, Z. Parsa, M. Stelts, and R. Chrien, in *Nuclear Cross Sections for Technology*, Vol. 594 of *NBS Special Publication*, edited by J. L. Fowler, C. H. Johnson, and C. D. Bowman, (Natl. Bur. Stand. (U.S.) Spec. Publ. No. 594 (U.S. GPO, Washington, D.C., 1979), p. 344.
- [15] S. Iijima, T. Watanabe, T. Yoshida, Y. Kikuchi, and H. Nishimura, in *Neutron Cross Sections of Fission Product Nuclei*, Vol. 209L of Report RIT/FISLDN(80) 1, NE-ANDC(E), edited by C. Coceva and G. Panini (CNEN, Bologna, 1979), p. 317.
- [16] H. Beer and F. Käppeler, *Phys. Rev. C* **21**, 534 (1980).
- [17] W. Ratynski and F. Käppeler, *Phys. Rev. C* **37**, 595 (1988).
- [18] S. Jaag (private communication).
- [19] *Handbook of Chemistry and Physics*, 53rd ed., edited by R. Weast (CRC Press, Cleveland, 1972), p. B-21.
- [20] E. der Mateosian and L. Peker, *Nucl. Data Sheets* **66**, 705 (1992).
- [21] J. Szucs, M. Johns, and B. Singh, *Nucl. Data Sheets* **46**, 1 (1985).
- [22] B. Singh, J. Szucs, and M. Johns, *Nucl. Data Sheets* **55**, 185 (1988).
- [23] R. Auble, *Nucl. Data Sheets* **40**, 301 (1983).
- [24] E. Storm and H. Israel, *Nucl. Data Tables* **36**, 375 (1970).
- [25] V. McLane, C. Dunford, and P. Rose, *Neutron Cross Sections* (Academic Press, New York, 1988), Vol. 2.
- [26] Z. Bao and F. Käppeler, *At. Data Nucl. Data Tables* **36**, 411 (1987).
- [27] H. Beer, F. Voss, and R. Winters, *Astrophys. J. Suppl.* **80**, 403 (1992).
- [28] J. Holmes, S. Woosley, W. Fowler, and B. Zimmerman, *At. Data Nucl. Data Tables* **18**, 305 (1976).
- [29] M. Harris, *Astrophys. Space Sci.* **77**, 357 (1981).
- [30] G. Reffo and Ge Zhigang (unpublished).
- [31] G. Reffo and F. Fabbri (unpublished).
- [32] K. Wisshak, J. Wickenhauser, F. Käppeler, G. Reffo, and F. Fabbri, *Nucl. Sci. Eng.* **81**, 396 (1982).
- [33] G. Reffo, F. Fabbri, K. Wisshak, and F. Käppeler, *Nucl. Sci. Eng.* **80**, 630 (1982).
- [34] P. Möller and R. Nix, technical report, Los Alamos National Laboratory (unpublished).
- [35] J. Mughabghab, M. Divadeenam, and N. Holden, *Neutron Cross Sections* (Academic Press, New York, 1981), Vol. 1, Pt. A.
- [36] J. Mughabghab, *Neutron Cross Sections* (Academic Press, New York, 1984), Vol. 1, Pt. B.
- [37] F. Käppeler, in *Radioactive Nuclear Beams*, edited by T. Delbar (Adam Hilger, Bristol, 1991), p. 305.
- [38] F. Käppeler, R. Gallino, M. Busso, G. Picchio, and C. Raiteri, *Astrophys. J.* **354**, 630 (1990).
- [39] M. Rayet, N. Prantzos, and M. Arnould, *Astron. Astrophys.* **227**, 271 (1990).
- [40] N. Prantzos, M. Hashimoto, M. Rayet, and M. Arnould, *Astron. Astrophys.* **238**, 455 (1990).
- [41] W. Howard, B. Meyer, and S. Woosley, *Astrophys. J.* **373**, L5 (1991).
- [42] S. Jaag and F. Käppeler, in *Nuclei in the Cosmos '94*, edited by M. Busso (AIP, New York, 1994).
- [43] I. Iben, Jr. and A. Renzini, *Annu. Rev. Astron. Astrophys.* **20**, 271 (1983).
- [44] D. Hollowell and I. Iben, Jr., *Astrophys. J.* **340**, 966 (1989).
- [45] R. Gallino, M. Busso, G. Picchio, C. Raiteri, and A. Renzini, *Astrophys. J.* **334**, L45 (1988).
- [46] R. Gallino, M. Busso, and C. Raiteri, in *Nuclei in the Cosmos '92*, edited by F. Käppeler and K. Wisshak (Institute of Physics, Bristol, 1993), p. 509.
- [47] S. Jaag, Master thesis, University of Karlsruhe, 1990.
- [48] R. Gallino (private communication).
- [49] E. Anders and N. Grevesse, *Geochim. Cosmochim. Acta* **53**, 197 (1989).
- [50] G. Lugmair, T. Shimamura, R. Lewis, and E. Anders, *Lunar Planet. Sci.* **14**, 448 (1983).
- [51] D. Clayton, *Astrophys. J.* **271**, L107 (1983).
- [52] E. Zinner, S. Amari, and R. Lewis, *Astrophys. J.* **382**, L47 (1991).
- [53] S. Richter, U. Ott, and F. Begemann, *Lunar Planet. Sci.* **23**, 1147 (1992).
- [54] S. Richter, U. Ott, and F. Begemann, in *Nuclei in the Cosmos '92*, edited by F. Käppeler and K. Wisshak (Institute of Physics, Bristol, 1993), p. 127.
- [55] F. Käppeler, H. Beer, and K. Wisshak, *Rep. Prog. Phys.* **52**, 945 (1989).
- [56] F. Käppeler, W. Schanz, K. Wisshak, and G. Reffo, *Astrophys. J.* **410**, 370 (1993).
- [57] F. Voss, K. Wisshak, K. Guber, F. Käppeler, and G. Reffo, *Phys. Rev. C* **50**, 2582 (1994).